Hindawi
Geofluids
Volume 2017, Article ID 6590672, 14 pages
https://doi.org/10.1155/2017/6590672

*Research Article*

# Ferroan Dolomitization by Seawater Interaction with Mafic Igneous Dikes and Carbonate Host Rock at the Latemar Platform, Dolomites, Italy: Numerical Modeling of Spatial, Temporal, and Temperature Data

**K. Blomme,[1] S. J. Fowler,[1] P. Bachaud,[2] F. H. Nader,[2] A. Michel,[3] and R. Swennen[1]**

[1]*Department of Earth and Environmental Sciences, KU Leuven, Leuven, Belgium*
[2]*Geosciences Division, IFP Energies Nouvelles, Rueil-Malmaison, France*
[3]*Mechatronics, Computer Science and Applied Mathematics Division, IFP Energies Nouvelles, Rueil-Malmaison, France*

Correspondence should be addressed to K. Blomme; katreine.blomme@kuleuven.be

Received 11 January 2017; Accepted 28 March 2017; Published 3 May 2017

Academic Editor: Timothy S. Collett



Numerous publications address the petrogenesis of the partially dolomitized Latemar carbonate platform, Italy. A common factor is interpretation of geochemical data in terms of heating via regional igneous activity that provided kinetically favorable conditions for replacement dolomitization. New field, petrographic, XRD, and geochemical data demonstrate a spatial, temporal, and geochemical link between replacement dolomite and local mafic igneous dikes that pervasively intrude the platform. Dikes are dominated by strongly altered plagioclase and clinopyroxene. Significantly, where ferroan dolomite is present, it borders dikes. We hypothesize that seawater interacted with mafic minerals, causing Fe enrichment in the fluid that subsequently participated in dolomitization. This hypothesis was tested numerically through thermodynamic (MELTS, Arxim-GEM) and reactive flow (Arxim-LMA) simulations. Results confirm that seawater becomes Fe-enriched during interaction with clinopyroxene (diopside-hedenbergite) and plagioclase (anorthite-albite-orthoclase) solid solutions. Reaction of modified seawater with limestone causes ferroan and nonferroan replacement dolomitization. Dolomite quantities are strongly influenced by temperature. At 40 to 80°C, ferroan dolomite proportions decrease with increasing temperature, indicating that Latemar dolomitization likely occurred at lower temperatures. This relationship between igneous dikes and dolomitization may have general significance due to the widespread association of carbonates with rifting-related igneous environments.

## 1. Introduction

Most dolomite forms when Mg-bearing aqueous fluid is transported through limestone, replacing calcite ($CaCO_3$) with dolomite ($CaMg(CO_3)_2$). A key question concerns the origin of the dolomitizing fluid. Geochemical data from fluid inclusions, stable C and O isotopes, Sr isotopes, and trace elements serve as widely used tracers in this regard because they provide information on composition, temperature, and fluid-rock ratios during dolomitization [1]. Dolomite is thermodynamically stable in seawater, which is overwhelmingly the most abundant Mg-bearing fluid; however, slow kinetics at ambient sea surface temperatures inhibits dolomitization. Elevated temperatures, generally attributed either to burial under the geothermal gradient, igneous activity, or deep hydrothermal fluid circulation, promote dolomitization [1, 2]. Reactive transport models have brought some insight into dolomitization [e.g., [3–7]]. Although they have so far provided important constraints on driving mechanisms for the transport of dolomitizing fluid and for understanding the locations of dolomite bodies, their capacity for distinguishing the source of dolomitizing fluid has not yet been fully explored, particularly from a thermodynamic perspective.

This study uses new observations to constrain reactive transport simulations aimed at investigating the origin of dolomitizing fluid at the Latemar carbonate platform,

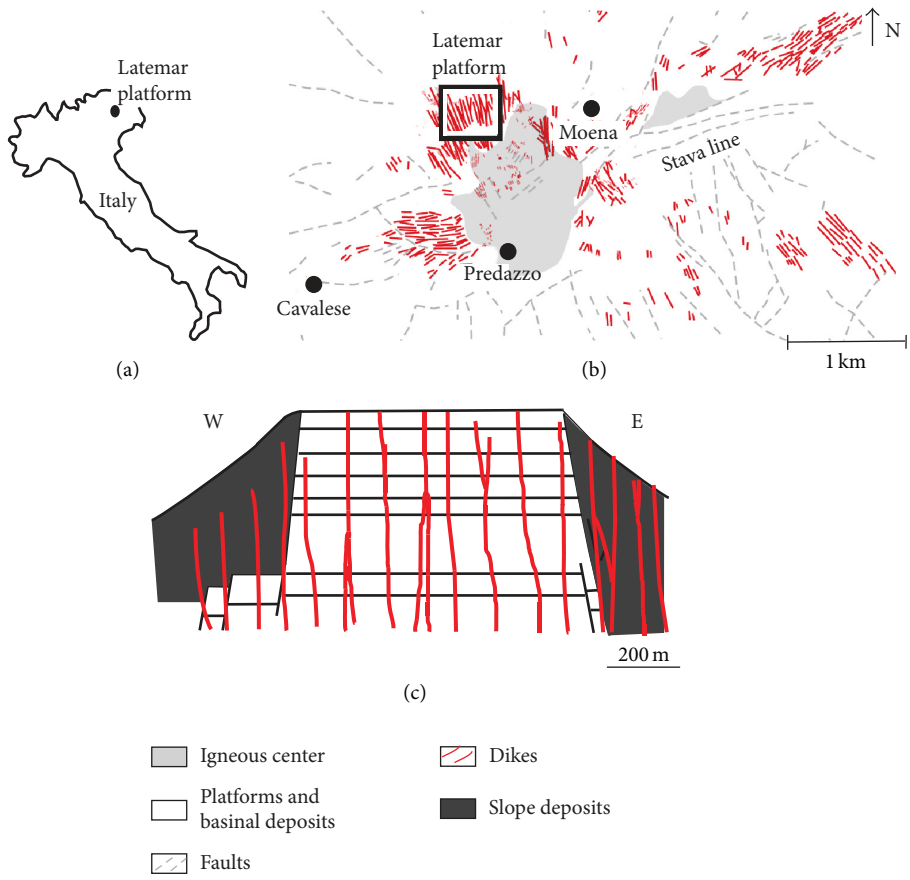


FIGURE 1: (a) Map showing the approximate location of the Latemar carbonate platform within northern Italy. (b) Simplified geological map of the Latemar platform (box) [8, 9] showing mafic dikes intruding the platform and related major intrusions of the Predazzo igneous complex. (c) Schematic E-W cross-sectional diagrams of Latemar platform highlighting dike geometry [10].

northern Italy (Figure 1(a)). Mafic, subvertical ~3 m-thick dikes pervasively crosscut the platform [8–10] (Figure 1). Latemar platform dolomite includes cycle cap and replacement varieties [10], of which only the volumetrically dominant replacement dolomite is considered here. Replacement dolomite is of ferroan and nonferroan type, often discernible in the field based on orange and tan color, respectively [11]. Replacement is of Middle Triassic (Anisian and Ladinian) limestone [11, 12]. Due to its excellent exposure, the Latemar platform has attracted intense attention as an analogue of a subsurface carbonate reservoir and a variety of published dolomitization scenarios now exist [10–14]. Based on interpretation of fluid inclusion salinities, stable isotope data, and Sr isotope data, the consensus is that seawater was a significant component of the dolomitizing fluid [10, 12, 13]. However, Carmichael and Ferry recognized that seawater has insufficient Fe to account for the presence of ferroan dolomite [13]. On a qualitative basis, they linked elevated dolomite Fe, Mn, and Zn concentrations with midocean ridge vent emissions derived from the Predazzo igneous complex near the Latemar platform (Figure 1(b)). Predazzo igneous activity overlapped temporally with Latemar platform dolomitization [232–238 Ma; [15, 16]], although there is no record of an associated midocean ridge environment during the mid-Triassic [17–19]. A link between Predazzo activity and dolomitization is also consistent with elevated dolomitization temperatures that exceed those associated with the geothermal gradient at the maximum platform burial depth of <1 km. Dolomitization temperatures have been measured most recently at 40 to 80°C based on clumped isotope thermometry [20]. Temperatures based on microthermometric analysis of fluid inclusions of up to 200°C have previously been reported by [12] but are unreliable due to potential stretching and/or leaking of the fluid inclusions. Further insight comes from studies by Jacquemyn and coworkers that involved examination of geometric relationships between Latemar platform lithologies. Field observations and geostatistical analysis of a digital outcrop model showed that dolomite roughly parallels dikes and is more abundant closer to dikes [10, 14]. Dolomite petrogenesis was not considered explicitly in the studies, but Fe-rich dolomitizing fluid was hypothesized to have been derived from sedimentary lithologies below the Latemar platform. Overall, the petrogenesis and significance of ferroan and nonferroan dolomite remain unquantified.

This study presents new field, petrographic, XRD, and geochemical data associated with Latemar platform dike-carbonate contacts. From an observational perspective, patterns of ferroan and nonferroan dolomite distribution related to individual dikes and compositional characterization of the igneous rocks are of novel interest. The data are used to define

spatial, temporal, and geochemical relationships between the dikes and replacement dolomite. Based on the data, an original dolomitization conceptual model is proposed and then quantitatively evaluated using a multisoftware numerical approach. In the model, Latemar dolomite petrogenesis entails alteration of a limestone host rock by fluid modified compositionally via initial interaction with warm mafic dikes. Model evaluation involves first calculating the thermodynamic properties and compositions of major dike mineral phases upon solidification. Next is equilibration of seawater with major dike minerals at published dolomitization temperatures. Compositionally modified seawater then interacts with limestone. Compared to published reactive transport-based studies [e.g., [3, 23, 24]], a technical advantage of the simulations is incorporation of both ferroan and nonferroan dolomite phases and of solid solution thermodynamic models of the major mafic igneous phases, clinopyroxene and plagioclase.

## 2. Material and Methodology

*2.1. Analytical Methods.* We made general observations of dike-carbonate contacts and collected 230 related dike and carbonate (replacement dolomite and dolomite veins) samples during two distinct summer field campaigns. Sample profiles extended from dike interiors up to 25 m into the host rock. The dikes have so far received little attention in the literature aside from their geometries [10, 14]. Further detail on the petrogenesis and alteration of the dikes will appear in a separate paper. Sample transects are provided in Appendix A in Supplementary Material available online at https://doi.org/10.1155/2017/6590672.

Thin sections were examined using transmitted-light optical microscopy (Leica microscope). Carbonate samples and thin sections were stained with a mixture of Alizarine Red S and K-ferricyanide [25] to differentiate calcite from dolomite and ferroan from nonferroan dolomite. Dike modes were determined via point counting and Jmicrovision software, which allows random point counting on photomicrographs to determine relative phase abundances.

The mineralogy of carbonate and dike samples was determined by X-ray diffraction (XRD) using a Philips PW1830 diffractometer with a Bragg/Brentano theta-2 theta setup and CuK radiation at 45 kV and 30 mA. The machine was equipped with a graphite monochromator. The receiving and divergence slit width was 1 mm and the antiscatter width was 0.1 mm. The resulting XRD diffractograms were analyzed qualitatively with the DiffracPlus (Eva) software.

Whole-rock dike oxide data were collected via Inductively Coupled Plasma-Optical Emission Spectroscopy (ICP-OES) at KU Leuven, Belgium, with a Varian ES ICP-OES Spectrometer. Samples were fused using the $LiBO_2$ method.

Detailed semiqualitative chemical point analyses were performed using a scanning electron microscope (SEM) equipped with an energy dispersive spectrometer (EDS). The beam voltage was set at 12 kV. Resulting spectra were analyzed using AZtecEnergy software (Oxford Instruments). These analyses are supported by electron microprobe analyses (EMPA) that provide quantitative mineral compositional data on carbonate phases. Measurements were carried out with a Cameca SX50 electron microprobe at the Department of Geology and Applied Geology, University of Mons, Belgium. The microprobe is equipped with four wavelength-dispersive spectrometers. Analyzing conditions for the carbon-coated samples were fixed at 15 kV and 20 nA.

*2.2. Modeling Software.* Simulations were performed with the MELTS [26, 27] and Arxim [28] software packages. MELTS is thermodynamically based software that performs phase equilibria calculations in magmatic systems (i.e., where silicate melt is present). A system may also contain crystals (including solid solutions) and supercritical fluid ($H_2O$). Arxim simulates reactions between multicomponent fluids and minerals based on either global Gibbs free energy minimization (Arxim-GEM) or a Law of Mass Action approach (Arxim-LMA). Arxim-GEM can predict compositions of stable solid solution phases and their thermodynamic properties for chemical systems defined in terms of elementary composition, temperature, and pressure. Arxim-LMA is restricted to fixed-composition phases that are identified a priori. Arxim-LMA has the advantage of allowing kinetic reactions and simple nondimensional reactive flow simulation, where a single host rock cell may react with fluid of specified composition injected at constant velocity.

## 3. Geological Characterization

*3.1. Field Observations.* Jacquemyn and coworkers [10] noted that Latemar platform dolomite is more abundant closer to dikes. We observed patterns in the relative distributions of ferroan and nonferroan dolomite (Figure 2(a)). Ferroan dolomite (where present) borders dikes, whereas nonferroan dolomite is located relatively further afield (Figures 2(a)–2(c)). On average, ferroan dolomite extends over distances of 0.5 to 2.5 m from dike-host rock contacts. For example, at the outcrop shown in Figure 2, only ferroan dolomite is present within 0.87 m of the dike-host rock contact. Ferroan dolomite is not present at further than 0.87 m from the contact. Nonferroan dolomite is present starting at 0.87 m from the contact. It extends away from the contact over a distance of 1.11 m. Ferroan dolomite outcrops are more common in the upper part of the Latemar platform than at the base, possibly because of better exposure of dike contacts and geometries near the top of the platform. In addition, ferroan dolomite veins crosscut the majority of dikes (Figure 3(a)). Neither ferroan nor nonferroan dolomite veins were observed crosscutting replacement dolomite.

*3.2. Dolomite Mineralogy and Major Elements.* Consistent with field observations, XRD spectra show that where ferroan dolomite is present, there is a sharp compositional change from ferroan to nonferroan dolomite with increasing distance from individual dikes. Figure 2(b) provides an example. Dolomite $d_{104}$ values range from 2.8853 to 2.8971 Å, corresponding to FeO concentrations of <0.5 to 10 wt.% (Appendix B). EMPA results reveal that dolomite veins crosscutting dikes have 0.20 Fe per formula unit (~10 wt.%), which is strikingly high compared to the maximum value

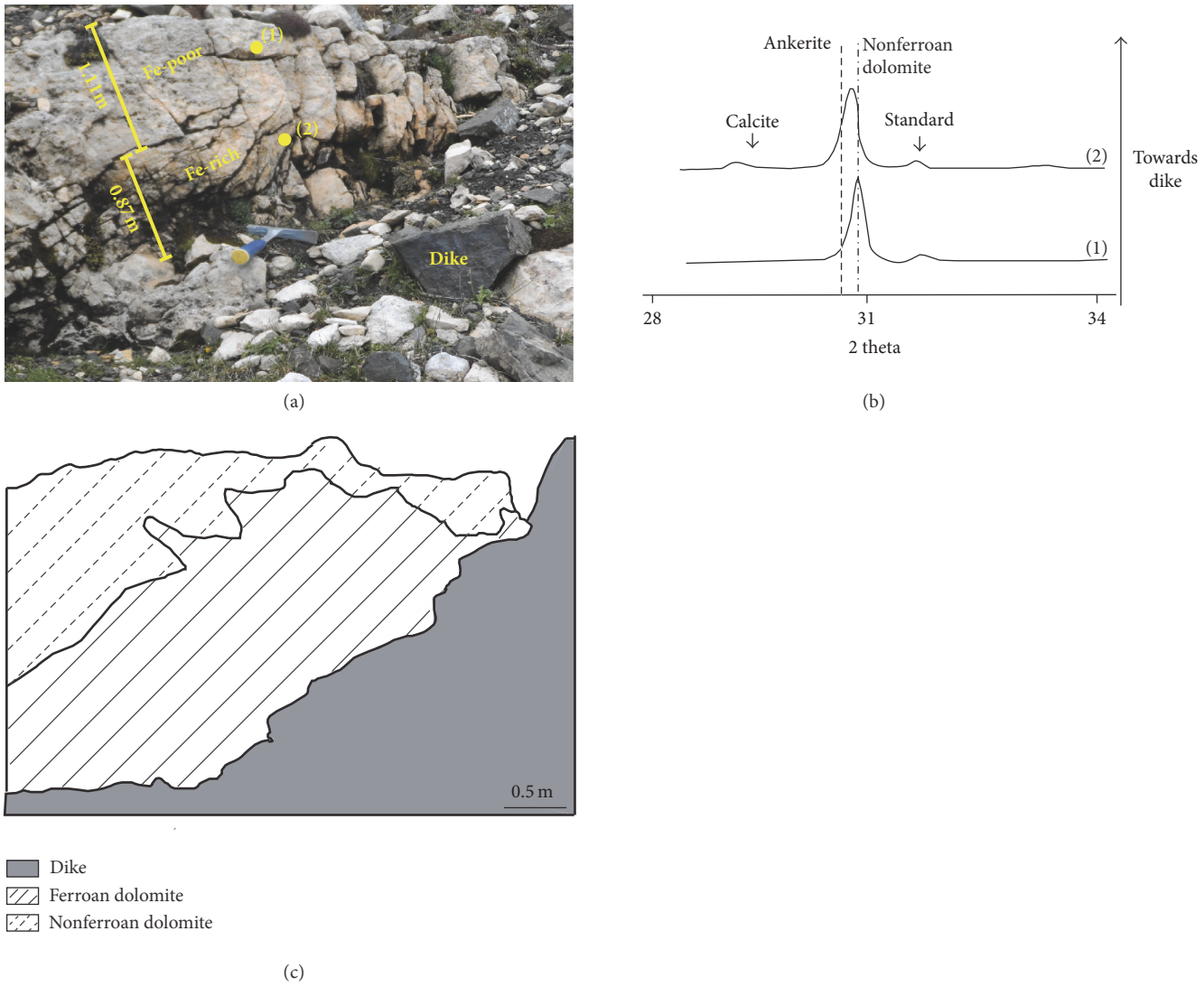


Figure 2: Summary of field observations (a) Dike-carbonate contact showing replacement ferroan dolomite bordering a dike. Here (and in general) ferroan dolomite occurs close to the dike, while nonferroan dolomite occurs further away from the dike. Numbers indicated in the figure correspond to XRD spectra shown in (2b). (b) XRD diffractograms based on samples from (2a), including nonferroan (1) and ferroan (2) dolomite. Sample locations are indicated in (2a). Towards the dike, there is a shift from nonferroan dolomite to ferroan dolomite. (c) Schematic interpretation of (2a).

of 0.07 Fe per formula unit (~2 wt.%) reported by [11] for ferroan replacement dolomite (Appendix C). As shown in Figure 3(b), dolomite veins can be seen crosscutting altered clinopyroxene crystals.

Figure 3(c) shows crystal-scale transitions between ferroan and nonferroan dolomite. Colorless nonferroan dolomite crystal rims have the same crystallographic orientations as their blue-stained ferroan dolomite cores. Colorless nonferroan dolomite also occurs as an intercrystalline cement phase between ferroan dolomite crystals.

*3.3. Dike Mineralogy and Major Elements.* Latemar dikes typically have seriate to (glomero)porphyritic textures. The major phenocryst phases are plagioclase (~18–60 vol.%; 28 vol.% on average) and clinopyroxene (~5–60 vol.%; 18 vol.% on average; Figures 3(d) and 3(e)). Most plagioclase crystals exhibit compositional zoning and have irregular rims, which may indicate, respectively, fractional crystallization and reaction within silicate melt (Figure 3(d)). Minor sanidine (up to ~5 modal%, Appendix D) and magnetite (trace) are present. The groundmass is micro- to cryptocrystalline (Figures 3(d)–3(i)). Only plagioclase is readily identifiable. All samples are strongly to moderately altered (Figures 3(b) and 3(f)–3(i)). Chlorite, sericite, smectite, and calcite are the most common alteration products based on petrography and XRD data (Appendix D). Care was taken during dike sampling to avoid collecting samples with the most obvious signs of alteration, such as green hues resulting from chloritization or cloudy feldspars.

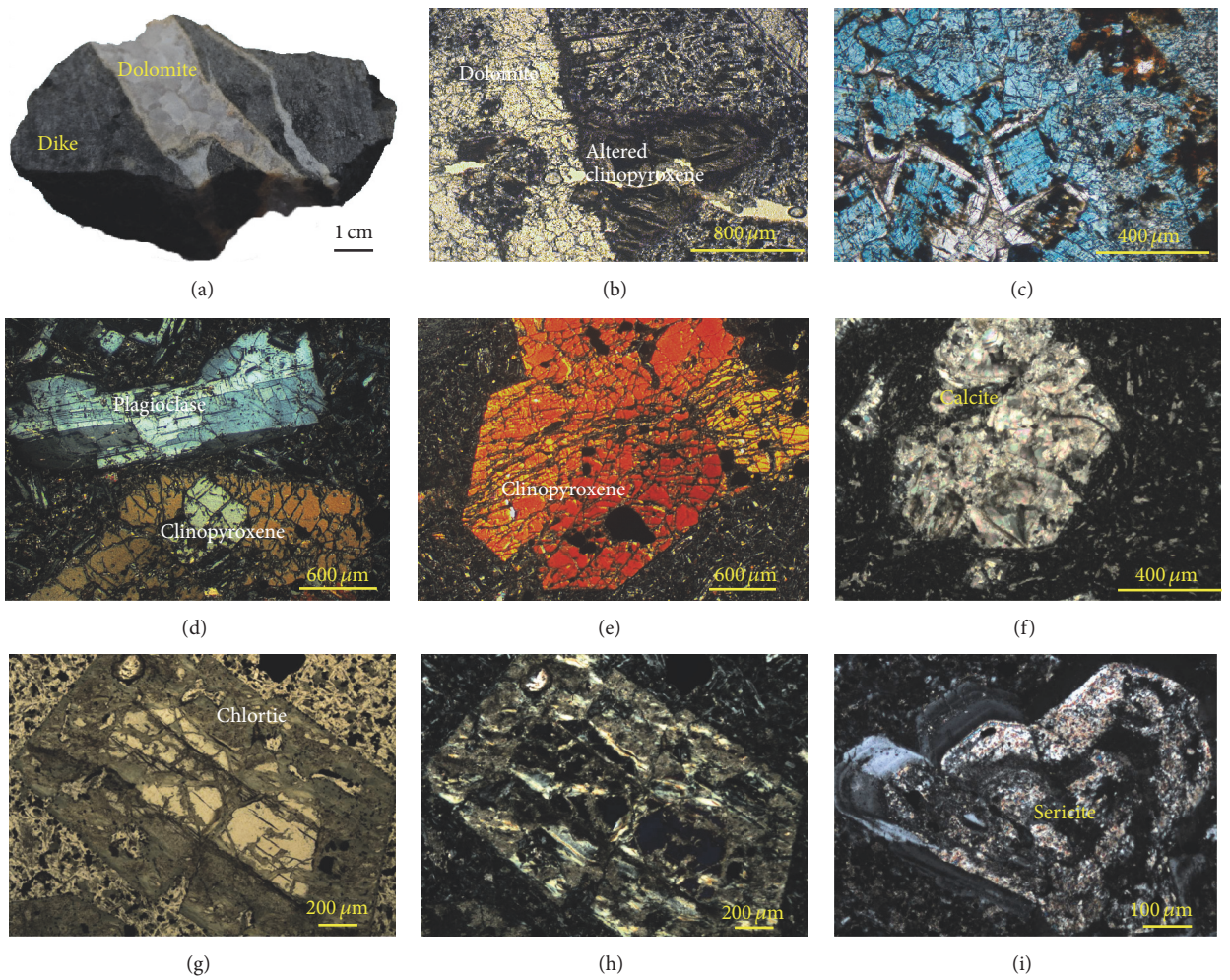


Figure 3: (a) Hand sample of a dolomite vein crosscutting a dike where the sample is unstained. (b) Photomicrograph (plane-polarized light (PPL)) of a dolomite vein crosscutting a reacted pyroxene crystal in a dike. (c) Photomicrograph (PPL) of a stained dolomite sample showing colorless-grey nonferroan dolomite as a cement phase filling pore space between blue-stained ferroan dolomite crystals. (d) Photomicrograph (cross-polarized light (XPL)) of plagioclase and clinopyroxene phenocrysts where the plagioclase is embayed. (e) Photomicrograph (XPL) of a clinopyroxene glomerocryst in a cryptocrystalline groundmass. (f) Photomicrograph (XPL) of a phenocryst that is completely altered to calcite in a cryptocrystalline groundmass. (g) Photomicrograph (PPL) of a clinopyroxene phenocryst that is altered to chlorite along its edges. At the center of the phenocryst, the original mineral can still be recognized. (h) XPL photomicrograph of (g). (i) Photomicrograph (XPL) of feldspar phenocrysts that have been altered to sericite.

Table 1 provides a dike whole-rock composition calculated by averaging ICP-OES analyses from eight samples. Based on major element data (Table 1), dikes are basaltic to basaltic trachyandesite.

We performed SEM-EDS point analyses (Figure 4) to investigate the effects of dike alteration on clinopyroxene chemistry. Figures 4(b) and 4(c) show SEM-EDS spectra corresponding, respectively, to unaltered and altered clinopyroxene. Based on the spectra, both samples can be classified as diopside (average composition $Di_{62}Hd_{38}$), where Fe, Mg, and, to a lesser extent, Ca have been leached during alteration. An additional transect is provided in Appendix E.

*3.4. Conceptual Model of Latemar Dolomitization.* Crosscutting relationships gleaned from field and petrographic data constrain the relative timing of dike alteration and ferroan

Table 1: Major element composition of Latemar dikes (average of eight samples).

| Oxide | Wt.% |
|---|---|
| $SiO_2$ | 44.31 ± 3.50 |
| $TiO_2$ | 1.10 ± 0.28 |
| $Al_2O_3$ | 16.60 ± 0.89 |
| MnO | 0.12 ± 0.04 |
| CaO | 9.66 ± 2.99 |
| $Na_2O$ | 2.09 ± 0.67 |
| $K_2O$ | 4.48 ± 2.24 |
| FeO | 8.76 ± 2.18 |
| MgO | 3.59 ± 1.85 |
| $P_2O_5$ | 0.32 ± 0.05 |

Analysis calculated on an anhydrous and $CO_2$-free basis. All Fe is represented as FeO.

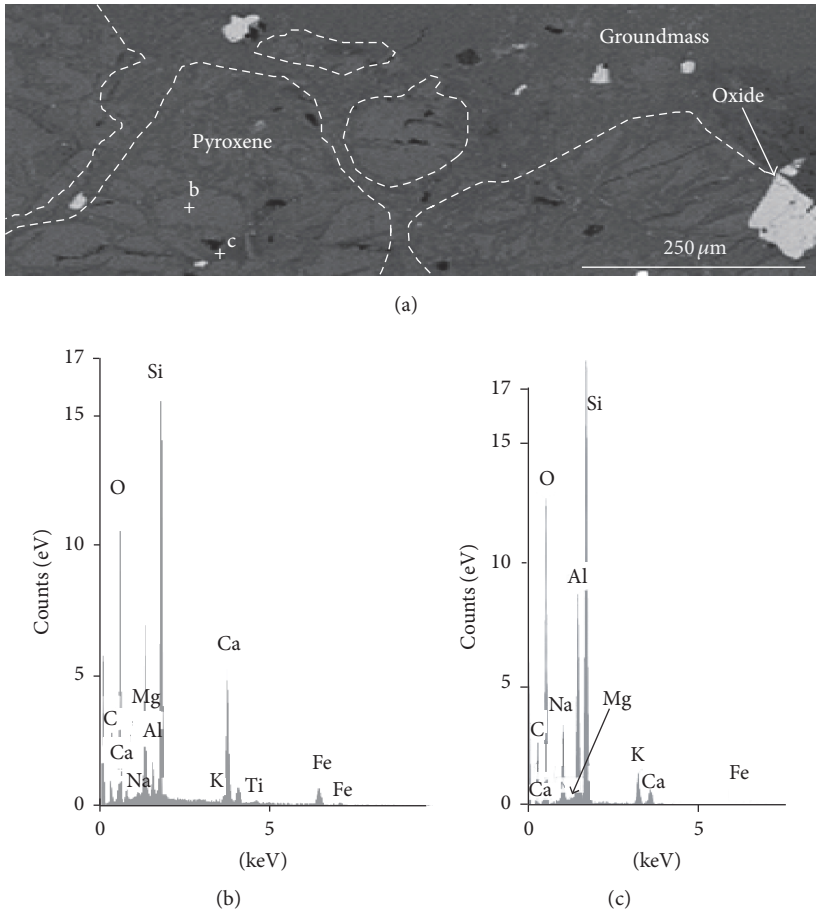


Figure 4: (a) Back-scattered electron image of an altered dike. White dashed lines trace clinopyroxene crystals. SEM-EDS spectra of (b) a dike clinopyroxene phenocryst and (c) a clinopyroxene alteration product, most likely a clay phase.

dolomitization. The dolomite veins that crosscut the majority of dikes show that dolomite postdates dike emplacement and solidification. Crosscutting of altered clinopyroxene by the veins shows that the clinopyroxene reacted prior to or contemporaneously with dolomite formation (Figures 3(a) and 3(b)). Dolomite Fe contents gradually decreased during dolomitization (Figure 3(c)), a relationship that can be explained through consecutive precipitation from a chemically evolving fluid whereby ferroan dolomite precipitated first. Maximum dolomite Fe concentrations are associated with the veins that crosscut the dikes and there is a spatial decrease in dolomite Fe concentrations away from dikes, further indicating that the ferroan phase formed prior to the nonferroan one. This is consistent with the paragenesis presented by [10].

Figure 5 summarizes our novel hypothesis for Latemar platform replacement dolomitization. During the mid-Triassic, the Predazzo igneous complex was active for ~6 Ma [15, 16], providing ample time for seawater circulation throughout the platform during submarine residence of the platform [12]. Pervasive dike intrusion led to heating of limestone host rock and favorable kinetic conditions for dolomitization local to dikes. Seawater interacted with and altered dikes in which (typical of basaltic lithologies) clinopyroxene was the most abundant mafic mineral. The product fluid, enriched in Fe, Mg, and possibly Ca, then reacted with limestone host rock. Ferroan replacement dolomitization consumed Fe close to dike contacts with host rock, providing a tangible physical record of the importance of magmatic heating for dolomitization at shallow crustal levels.

A key point is that the Fe component of ferroan dolomite was sourced locally from the Latemar dikes. This is consistent with alteration of the dikes and with the spatial relationship between ferroan dolomite and the dikes. Jacquemyn et al. [10] suggested that the Fe-rich fluids were derived from below the Latemar platform by flow along permeable brecciated contacts between limestone and dikes. Our detailed observations have revealed that brecciated dike margins form a minority of contacts (<10%), whereas fractures extending across contacts are common. Also, the presence of altered juvenile minerals and hydrous secondary minerals in the dikes shows that brecciation is not required to make dikes sufficiently permeable for fluid circulation. More importantly, we know of no likely sources of Fe below the Latemar platform. The Val Gardena sandstone, which lies stratigraphically below the Latemar platform, is Fe-bearing. However, according to [10],

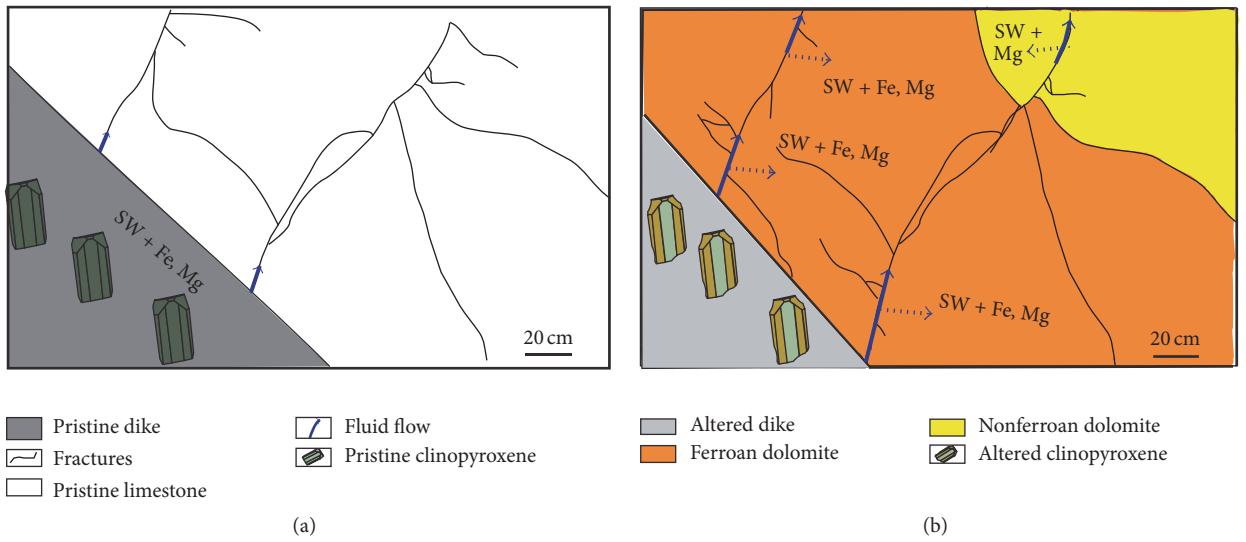


Figure 5: Summary of the proposed conceptual model of Latemar dolomitization. (a) Onset of dolomite formation. Seawater becomes enriched in Fe and Mg during interaction with mafic dike minerals. (b) When this modified seawater composition interacts with platform limestone, ferroan and nonferroan dolomite replace limestone.

its Sr isotopic signatures are more radiogenic than Latemar replacement dolomite, which has a Sr isotopic range of 0.70730 to 0.70800. Permian basement is much less mafic than the Latemar dikes. It is therefore unlikely to have provided sufficient Fe for ferroan dolomitization. Also, its Sr isotope values of 0.7599 to 0.7656 at 235 Ma [17, 18] are significantly higher than those of the replacement dolomite. It is worth noting that some Latemar replacement dolomite Sr isotopic values are slightly depleted compared to Triassic seawater (0.70755 to 0.70820 [10, 29]). Initial dike Sr isotopic values range from 0.70401 to 0.70600 [10]. Interaction of seawater with dikes would therefore be generally consistent with the Sr isotopic signatures of replacement dolomite.

The major Predazzo igneous complex, the likely source of the Latemar dikes, may have provided heat and fluid to the Latemar platform. Due to the unknown volume and magma recharge history of the Predazzo igneous complex and the complex and poorly constrained permeability structure of Latemar area country rock, it is not feasible to discern via quantitative modeling whether fluid circulation from the Predazzo complex may have influenced Latemar dolomitization. However, we suggest that the association of Latemar dolomite (and ferroan dolomite in particular) with dikes and the alteration of dikes indicate that the dikes were of dominant importance during dolomitization.

## 4. Modeling Seawater-Dike Interaction and Dolomitization

*4.1. Modeling Strategy.* Evaluation of the validity of our dolomitization conceptual model is based on numerical simulations with three geochemical codes (Figure 6). Due to the altered nature of many dikes, we first used MELTS to verify the types and proportions of minerals formed during dike solidification. Solidification simulations proceeded via fractional crystallization (as opposed to equilibrium crystallization) for consistency with petrographic observations such as plagioclase zoning. Next was calculation of the stable dike mineral assemblage at the pressure and calculated temperature (from MELTS) of dike solidification in Arxim-GEM, followed by comparison of MELTS and Arxim-GEM results. In addition, Arxim-GEM was used to calculate the thermodynamic properties (in the form of mineral equilibrium constants) at dolomitization temperatures for the major predicted dike phases. Calculated solid solution compositions and associated thermodynamic data served to enhance the database used for subsequent Arxim-LMA simulations. Arxim-LMA simulations used new fixed-composition species corresponding to the pristine dike assemblage. Arxim-LMA modeling aims (Figure 6) involved predicting the evolution of fluid composition during interaction between dikes and seawater and then calculating the amounts of ferroan and nonferroan dolomite formed by reaction of modified seawater with limestone (dike-host rock).

In particular, the modified seawater composition was calculated by buffering seawater with major dike phases (clinopyroxene and plagioclase solid solutions), meaning that the fluid was allowed to achieve equilibrium with the dike phases. Formation of secondary dike minerals was not considered in this initial study; this is addressed, however, in separate work on dike petrogenesis as mentioned in Section 2. The maximum amount of Fe available to form ferroan dolomite was delimited by the solubility of Fe-bearing clinopyroxene solid solution, while Al was constrained by feldspar dissolution.

A subsequent step consisted of injecting modified seawater into a single-celled host rock. For comparison purposes, we repeated this step with unmodified seawater, meaning present-day seawater not reacted with dikes. Further detail

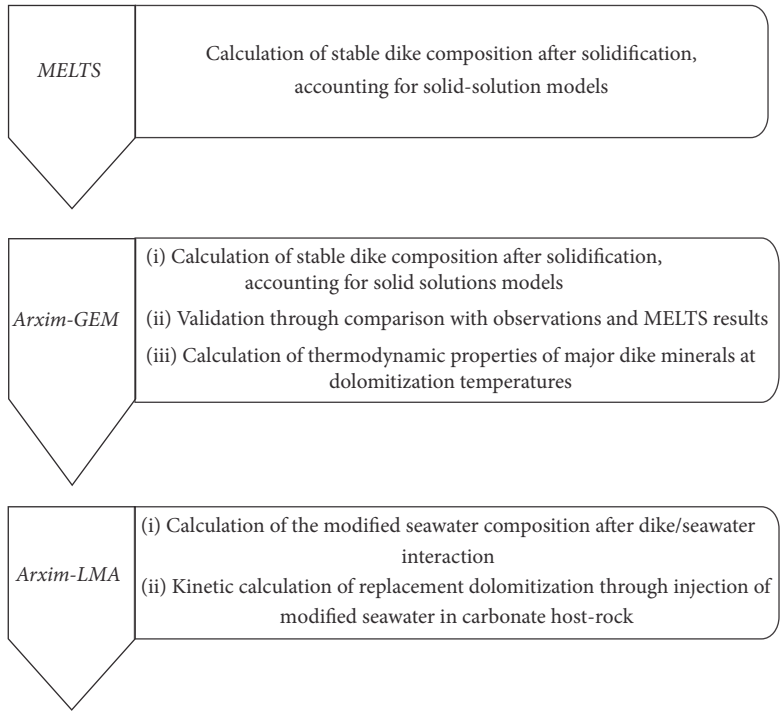


Figure 6: Overview of simulation workflow.

regarding the seawater compositions is presented in the next section. Mineral reactions occurred under kinetic constraints and, similar to [24], all simulations were isothermal. We did not consider transient temperature evolution due to heating of host rock or cooling of dikes following dike intrusion. An individual dike would likely have solidified via pure conduction within a few years. However, due to the dense nature of dike intrusion, fluid circulation throughout the platform (as evidenced by the occurrence of secondary hydrous minerals within the dikes), and the unknown contribution of heat from the Predazzo igneous complex (of unknown volume, magma recharge history, and crystallization-related latent heat contribution [30]), it is not straightforward to predict platform temperature evolution following dike intrusion.

*4.2. Modeling Inputs and Constraints.* MELTS inputs for simulation of magma solidification come from whole-rock oxide data collected via ICP-OES analysis of Latemar dikes, where parent magma corresponds to samples with relatively higher wt.% MgO (Table 1), and a pressure and temperature range for solidification. Latemar dikes are subvertical and pressures during solidification likely ranged from <0.05 to ~0.1 GPa based on observed platform thickness and estimates of burial thickness [12]. Simulation of solidification began at the calculated liquidus temperature and proceeded according to decreasing temperature via fractional crystallization. Simulation was terminated at ~1105°C, where phase assemblage predictions coincided with petrographic observations. Pressure, a parameter with a generally minor impact on the stability of mafic mineral phases at upper crustal conditions, was fixed at a constant value of 0.1 GPa.

The Arxim-GEM input composition also corresponds to dike whole-rock oxide data from ICP-OES analysis. Arxim-GEM was not used to model the process of dike solidification. A dike stable mineral assemblage was calculated at 1105°C and 0.1 GPa and then compared with MELTS results for validation. The thermodynamic properties of the calculated phases were then evaluated at 40, 60, and 80°C, spanning the most recently published range of dolomitization temperature for the Latemar platform [20]. The Arxim-GEM thermodynamic database is based on [31] and solid solution activity models for dike minerals come from [32, 33].

All Arxim-LMA simulations use the Debye-Hückel activity model for seawater [21, 34] and thermodynamic data from the SLOP98 database for aqueous species, nonferroan dolomite, and calcite [35, 36]. Due to the absence of a solid solution model for ferroan dolomite, its thermodynamic properties were simulated by a mechanical mixture of 94% disordered dolomite and 6% ankerite [11, 13, 37]. The composition of unmodified present-day seawater is presented in Table 2 [21, 22]. Secular variations in seawater composition may influence replacement dolomitization potential; Triassic seawater has a lower Mg-Ca ratio than modern seawater and therefore has a lower dolomitization potential. Despite significant uncertainty associated with its composition [21, 22], we performed a simulation based on Triassic seawater instead of modern seawater for comparison purposes. Table 2 presents calculated major component speciation for both seawater compositions at 25°C and 0.1 MPa. Elementary compositions and constraints used for the calculations come from [13, 21, 22].

Table 2: Major component speciation of present-day and Triassic seawater at 25°C and 0.1 MPa.

| Species | mol/kg $H_2O$ | pH |
|---|---|---|
| | Present-day seawater | |
| $Ca^{+2}$ | $1.03 \cdot 10^{-2}$ | 8.43 |
| $K^{+}$ | $1.02 \cdot 10^{-2}$ | |
| $Mg^{+2}$ | $5.31 \cdot 10^{-2}$ | |
| $Na^{+}$ | 0.468 | |
| $SO_4^{-2}$ | $2.8 \cdot 10^{-2}$ | |
| $SiO_2$(aq) | $9.99 \cdot 10^{-5}$ | |
| $Cl^{-}$ | 0.546 | |
| $Fe^{+2}$ | $1.00 \cdot 10^{-6}$ | |
| $Al^{+3}$ | $3.71 \cdot 10^{-8}$ | |
| $HCO^{-3}$ | $2.36 \cdot 10^{-3}$ | |
| | Triassic seawater | |
| $Ca^{+2}$ | $3.05 \cdot 10^{-2}$ | 8.10 |
| $K^{+}$ | $1.44 \cdot 10^{-2}$ | |
| $Mg^{+2}$ | 0.11 | |
| $Na^{+}$ | 0.48 | |
| $SO_4^{-2}$ | $2.80 \cdot 10^{-2}$ | |
| $SiO_2$(aq) | $1.23 \cdot 10^{-4}$ | |
| $Cl^{-}$ | 0.73 | |
| $Fe^{+2}$ | $1.00 \cdot 10^{-6}$ | |
| $Al^{+3}$ | $2.00 \cdot 10^{-6}$ | |
| $HCO^{-3}$ | $2.36 \cdot 10^{-3}$ | |

Fluid speciation was calculated in Arxim-LMA. For present-day seawater, input values from [21] were used. For Triassic seawater, Ca/Mg and metal concentrations were taken from [13]. Other values correspond to values from [22].

The initial platform mineralogy corresponds to calcite with negligible, but equal amounts of ferroan and nonferroan dolomite (<1%), as kinetic calculations in LMA-based codes require definition of secondary minerals in initial seed quantities. Consistent with Arxim-GEM simulations, Arxim-LMA simulations were run at system temperatures of 40, 60, and 80°C and a constant pressure of 0.02 GPa, corresponding to dolomitizing conditions at the Latemar platform. The initial porosity was 8%. Sensitivity tests were run at minimum porosities of 0.9%, based on data from Latemar limestone provided by [11]. The fluid injection rate was a constant 1 m/y based on values presented by [5] for geothermal convection of seawater in a carbonate platform. The following discussion refers to the 1 m/y rate as the "baseline case." Similar to [24], we ran additional calculations at minimum and maximum rates of 0.1 and 10.0 m/y, respectively, to investigate the influence of variations in flow rate on dolomitization. The reactive surface area (RSA) for calcite, ferroan dolomite, and dolomite was set at a baseline case value of 5300 $cm^2/g$, corresponding to grain diameter of 4 $\mu$m. Additional simulations were run to explore the effects of decreasing the RSA to 530 $cm^2/g$ (grain diameter of 40 $\mu$m) and 53 $cm^2/g$ (grain diameter of 400 $\mu$m), thereby covering the range of crystal sizes of the various carbonate fractions measured at the Latemar platform [10]. The activation energy and kinetic rate constant for calcite correspond to those from the USGS compilation [38] and are, respectively, equal to $2.35 \cdot 10^4$ J/mol and $1.549 \cdot 10^{-6}$ $mol/m^2s$. Dolomite kinetic parameters are more difficult to constrain, as very few data are available in the literature for precipitation rates. One of the rare published parameter sets is derived from the high-temperature experiments of [2], used for instance by [24]. Data from these experiments have been acquired for ordered dolomite. Latemar ferroan and nonferroan dolomite are thermodynamically closer to disordered dolomite, which is associated with a higher reaction rate than ordered dolomite [38]. As other studies, including [23], have used faster dolomite kinetics, we made the modeling choice of increasing the kinetic rate constant proposed by [2] by a factor of 10000 (thus staying well within the range used in [23]). The kinetic parameters used for ferroan and nonferroan dolomite in our baseline scenario therefore include an activation energy of $1.335 \cdot 10^5$ J/mol and a kinetic rate constant at 25°C of $4.585 \cdot 10^{-15}$ $mol/m^2s$. The impact of these parameter values on the dolomitization reaction was investigated further by lowering the kinetic rate constant to $4.585 \cdot 10^{-19}$ $mol/m^2s$, which corresponds to the value used in [2].

*4.3. Baseline Simulation Results.* MELTS simulations, performed under the conditions described above, confirm that clinopyroxene and plagioclase were the dominant stable mineral phases following dike solidification (Table 3). Calculated clinopyroxene compositions are diopside ($Di_{80}Hd_{20}$ to $Di_{68}Hd_{32}$). They encompass measured SEM-EDS data ($Di_{62}Hd_{38}$) reported in Section 3.3. Predicted plagioclase compositions are anorthitic ($An_{92}Ab_{07}Or_{01}$ to $An_{83}Ab_{15}Or_{02}$). Minor phases (<10% of the predicted phase assemblage) include sanidine, spinel, apatite, and olivine. There is no predicted exsolved supercritical fluid phase.

Table 3 presents the solid solution compositions predicted by Arxim-GEM for clinopyroxene and plagioclase at solidification conditions, along with the associated thermodynamic equilibrium constants calculated at the three investigated dolomitization temperatures. Overall, the predicted compositions for the two major dike minerals are comparable to the MELTS results: the clinopyroxene calculated formula unit falls well within the range estimated by MELTS. While a small discrepancy is observed on the feldspar solid solution, we deem it to be acceptable due to the inherent differences between the two codes, such as in their thermodynamic databases.

Table 4 shows the effect of seawater-dike interaction on the concentrations of species that are relevant to our concept. Following seawater-dike interaction, the amount of Fe in solution is higher than before interaction by an amount that depends on temperature. At 40°C, Fe shows an increase of 0.28 mmol/kg, while at 80°C, it is limited to 0.13 mmol/kg. This pattern is consistent with the decreasing solubility of most minerals with increasing temperature. Table 4 also compares the saturation index of the main system carbonates calculated before and after fluid interaction. Unmodified and modified seawater show higher values for nonferroan and ferroan dolomite than for calcite, indicating that both fluids

Table 3: Summary of the Arxim-GEM results. Log $K$ correspond to equilibrium constants of formation.

| Phase | MELTS-compositional range during cooling | Arxim-GEM composition during solidification | Log $K$ at 40°C | Log $K$ at 60°C | Log $K$ at 80°C |
|---|---|---|---|---|---|
| Feldspar | $An_{92}Ab_{07}Or_{01}$ to $An_{83}Ab_{15}Or_{02}$ | $An_{77}Ab_{22}Or_{01}$ | 655.99 | 617.34 | 583.10 |
| Clinopyroxene | $Di_{80}Hd_{20}$ to $Di_{68}Hd_{32}$ | $Di_{75}Hd_{25}$ | 490.21 | 461.31 | 435.73 |

Table 4: Comparison of the initial present-day seawater composition to the modified seawater composition (i.e., following dike alteration) at 0.02 GPa and 40°C, 60°C, and 80°C. Only the species relevant to the dolomitization conceptual model are presented. More detailed speciation results are presented in Appendix F.

| Temperature (°C) | Initial | | | Postseawater-dike interaction | | |
|---|---|---|---|---|---|---|
| | 40 | 60 | 80 | 40 | 60 | 80 |
| *Species (mole/kg)* | | | | | | |
| $Ca^{+2}$ | $1.03 \cdot 10^{-2}$ | $1.03 \cdot 10^{-2}$ | $1.03 \cdot 10^{-2}$ | $1.03 \cdot 10^{-2}$ | $1.03 \cdot 10^{-2}$ | $1.03 \cdot 10^{-2}$ |
| $Mg^{+2}$ | $5.31 \cdot 10^{-2}$ | $5.31 \cdot 10^{-2}$ | $5.31 \cdot 10^{-2}$ | $5.31 \cdot 10^{-2}$ | $5.31 \cdot 10^{-2}$ | $5.31 \cdot 10^{-2}$ |
| $Fe^{+2}$ | $1.00 \cdot 10^{-6}$ | $1.00 \cdot 10^{-6}$ | $1.00 \cdot 10^{-6}$ | $2.84 \cdot 10^{-4}$ | $1.64 \cdot 10^{-4}$ | $1.30 \cdot 10^{-4}$ |
| *Saturation index* | | | | | | |
| Calcite | 0.78 | 0.84 | 0.87 | 1.08 | 0.92 | 0.80 |
| Nonferroan dolomite | 2.08 | 2.39 | 2.62 | 2.68 | 2.56 | 2.49 |
| Ferroan dolomite | 2.04 | 2.34 | 2.56 | 2.79 | 2.64 | 2.56 |

can participate in dolomitization. Prior to reaction, nonferroan dolomite shows the highest saturation index; following reaction, ferroan dolomite is the most likely mineral to form at the three investigated temperatures.

Figure 7 summarizes the results of the Arxim-LMA simulations of modified seawater injection into limestone host rock under the conditions described above. Figure 7(a) presents the temporal evolution of calcite and total (ferroan and nonferroan) dolomite amounts and porosity during replacement dolomitization at 40°C. At this temperature, complete calcite replacement results in a small porosity increase. The reaction lasts approximately 10 ka, corresponding to a dolomitization rate close to $10^{-4}$ m/y. At temperatures of 60°C and 80°C, dolomitization rates increase to $6.67 \cdot 10^{-4}$ m/y and $1.67 \cdot 10^{-3}$ m/y, respectively. A comparable increase has been reported by [24] for a temperature range of 20 to 40°C.

Figure 7(b) shows ferroan and nonferroan dolomite proportions replacing calcite at the three temperatures of interest. The figure reveals a strong temperature control on the ratio of ferroan to nonferroan replacement dolomite. The predicted amount of replacement ferroan dolomite is considerably lower at 80°C than at 40°C; it represents 10% of platform minerals at 80°C compared to 80% of platform minerals at 40°C. In light of our field observations, these results indicate that Latemar dolomitization temperatures were likely closer to the lower end of the investigated temperature range.

*4.4. Discussion and Sensitivity Tests.* MELTS phase equilibria calculation of dike solidification does not lead to magmatic supercritical fluid exsolution; hence we conclude that midocean ridge vent emissions, as hypothesized by Carmichael and Ferry [13], do not form a likely dolomitizing fluid. In the fluid-rock interaction simulations, major igneous phases (clinopyroxene and plagioclase) have been simulated as solid solutions, a significant technical advance. However, the absence of a solid solution model for ferroan dolomite has required us to approximate ferroan dolomite as a mechanical mixture. This restricts the amount of Fe in the mineral. To aid in evaluating the impact of this approximation on our results, we performed simulations of modified modern seawater injection into limestone based on pure ankerite as the secondary mineral (i.e., instead of the mechanical mixture). Ankerite data come from [37], which uses the pure $CaFe(CO_3)_2$ endmember. All other input parameters are identical to the baseline case. Resulting platform mineral types and proportions after replacement at 40, 60, and 80°C are shown in Figure 8. Ankerite stability displays a dependence on temperature comparable to that of ferroan dolomite. This lends support to the notion that the temperature dependence of ferroan dolomite abundance is not an artifact related to the use of a mechanical mixture model. A second potential drawback of using a mechanical mixture compared to a solid solution is that it might somewhat underestimate the stability of ferroan dolomite [39] and therefore lead to an underestimation of the total amount of dolomite.

As described in Section 4.2, we also investigated the potential of modified Triassic seawater and unmodified (prior to reaction with dikes) modern seawater to form ferroan dolomite. Results of the corresponding 40°C reactive flow-based simulations are presented in Figure 9(a). The proportion of ferroan to nonferroan dolomite formed with modified Triassic seawater is equivalent to that based on modified

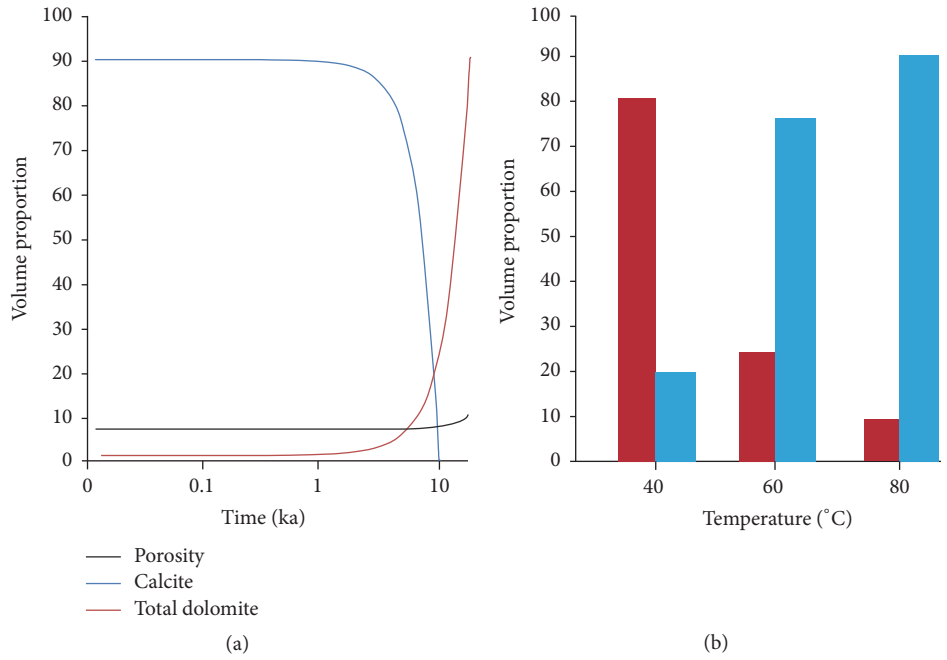


Figure 7: (a) Temporal evolution of calcite, total dolomite, and porosity during replacement dolomitization at 40°C. (b) Comparison of ferroan and nonferroan dolomite formed during injection of modified seawater into limestone host rock.

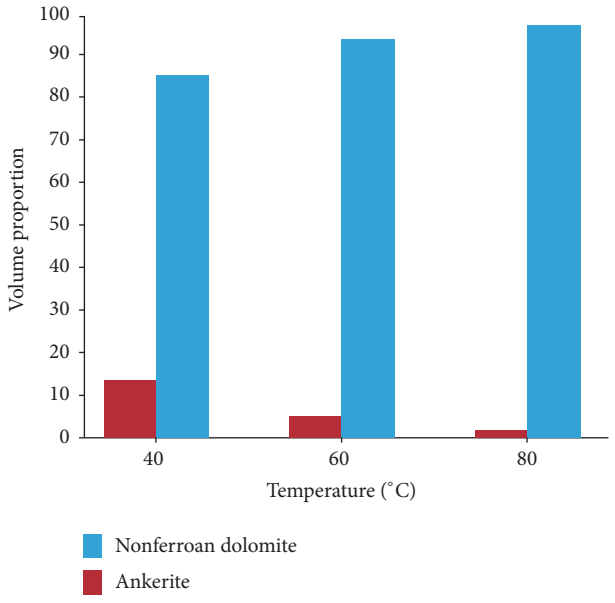


Figure 8: Comparison of ferroan and nonferroan dolomite generated via reactive flow of product fluid resulting from interaction of modern seawater with model dikes through calcite at 40, 60, and 80°C. Inputs and constraints correspond to the baseline case presented in Figure 7(b), with the exception that pure ankerite ($CaFe(CO_3)_2$) is considered instead of ferroan dolomite.

modern seawater. In contrast, unmodified present-day seawater does not allow the formation of ferroan dolomite. These results show that the initial fluid composition (most notably, its Fe to Mg ratio) is of secondary importance compared to the buffering effect of seawater reaction with dikes.

To evaluate the robustness of our simulations, additional sensitivity tests have been conducted on the least well-constrained parameters. Influences of platform initial porosity (Figure 9(b)), fluid injection rate (Figure 9(c)), mineral reactive surface area (Figure 9(d)), and kinetic rate constant of dolomite precipitation (Figure 9(e)) on platform dolomitization have been investigated. Results presented in Figure 9 are restricted to a temperature of 40°C.

From the results, we conclude that the parameters of interest have a restricted influence on the proportion of ferroan to nonferroan dolomite. The parameter with the greatest impact appears to be the injection flow rate. When set to 0.1 m/y, the predicted ferroan and nonferroan dolomite amounts are almost equal (52% and 48% of the platform mineral volume, resp.). The other parameters either have little overall influence (e.g., the initial platform porosity) or hinder dolomitization at their lowest input values. This is the case for the kinetic controls on dolomite precipitation, the reactive surface area and the kinetic rate constant (Figures 9(d) and 9(e)). As the injected fluid is supersaturated with respect to calcite (cf. Table 4) and as calcite has faster reaction kinetics than dolomite, secondary calcite can form, thereby inhibiting dolomite formation. As dolomitization is observed at the Latemar platform, these scenarios must be excluded. Ferroan dolomite remains the most abundant secondary mineral in the cases investigated, demonstrating the robustness of the calculations and supporting our conceptual model.

In contrast, the parameters do have a significant influence on the dolomitization rate, which varies between $1.4 \cdot 10^{-8}$

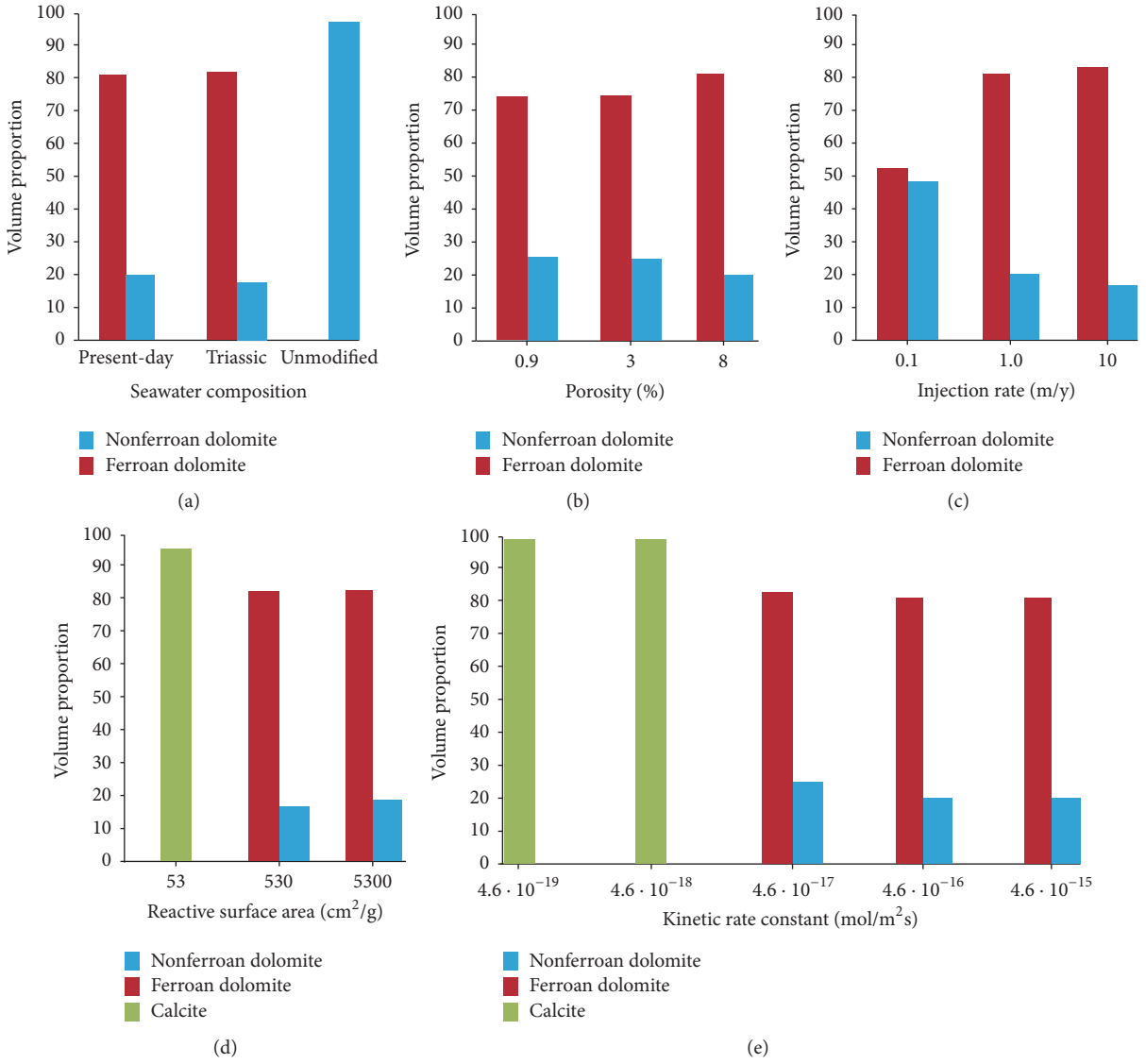


Figure 9: Overview of the sensitivity tests results. All results were obtained at 40°C. (a) Influence of the injected fluid composition. Unmodified seawater corresponds to present-day seawater before dike interaction. Present-day seawater corresponds to the baseline simulation. (b) Influence of the initial porosity. The 8% value corresponds to the baseline simulation. (c) Influence of the injection rate. The 1 m/y value corresponds to the baseline simulation. (d) Influence of the mineral reactive surface area. The 5300 $cm^2/g$ value corresponds to the baseline simulation. (e) Influence of kinetic rate constant of nonferroan and ferroan dolomites. The $4.6 \cdot 10^{-15}$ $mol/m^2s$ value corresponds to the baseline case.

and $1 \cdot 10^{-3}$ m/y. This variation is mainly due to variation in reactive surface area and kinetic rate constant. As Triassic seawater has a lower dolomitizing potential than present-day seawater, the associated dolomitization rate is lower ($9 \cdot 10^{-5}$ m/y versus $10^{-4}$ m/y, resp.). In contrast, decreasing the porosity does not significantly affect the dolomitization rate: at 3% porosity, the rate is still $0.95 \cdot 10^{-4}$ m/y. Aside from influencing the amount of ferroan to nonferroan dolomite, decreasing the fluid injection rate from 1 m/y to 0.1 m/y also decreases the dolomitization rate by two orders of magnitude (from $10^{-4}$ to $5.4 \cdot 10^{-6}$), which is well within the range proposed by [7].

## 5. Conclusion

A variety of observations (field, petrographic, XRD, and geochemical data) demonstrate spatial and geochemical relationships between igneous dikes and ferroan and nonferroan dolomite at the Latemar carbonate platform, Italy. Significantly, ferroan dolomite, where present, is restricted to dike-host rock contact areas. Nonferroan dolomite occurs further away from the dikes. SEM-EDS data reveal postsolidification alteration of clinopyroxene in dikes that released Fe and Mg, providing a source for ferroan dolomite. Crosscutting relationships show that ferroan dolomite was the first dolomite phase to precipitate. Based on these observations, we propose

a new conceptual model for Latemar dolomitization. The key point is that the Fe component necessary for ferroan dolomite formation was sourced locally by seawater interaction with dike minerals.

We tested the validity of our conceptual model through numerical simulations. The first modeling step consisted of incorporating solid solution models for the two major dike minerals, clinopyroxene and plagioclase. Their compositions and thermodynamic properties at solidification conditions were constrained using MELTS and Arxim-GEM software. Equilibration of seawater with these minerals was achieved using the Arxim-LMA code. The simulations show that seawater-dike interaction resulted in an increase of Fe in solution up to 0.28 mmol/kg. This enrichment is sufficient to cause the formation of ferroan dolomite during injection of the modified seawater into carbonate host rock. Ferroan and nonferroan dolomite quantities obtained during dolomitization are strongly dependent on temperature, a relationship that helps to constrain dolomitization conditions at the Latemar platform. Indeed, the simulations clearly demonstrate that the amount of ferroan dolomite decreases as temperature rises from 40 to 80°C; at 40°C it represents 80 vol.% of the initial calcite, while at 80°C this value drops to a mere 10%. Comparison of these numerical results with field observations indicates that the dolomitization temperature was therefore likely closer to the lower end of the examined range. Sensitivity tests demonstrate the robustness of the conceptual model. Model parameter values have very little impact on the proportion of predicted ferroan to nonferroan dolomite. In contrast, the dolomitization rate is highly sensitive, with values ranging from about $1.4 \cdot 10^{-8}$ m/y to $1 \cdot 10^{-3}$ m/y, depending mostly on reactive surface area, kinetic rate constant, and injection rate.

These results demonstrate advantages of comparing quantitative predictions from thermodynamically oriented reactive flow simulations with spatially constrained geochemical data from a natural system. For example, parameters such as temperature and the controls of reaction kinetics can be constrained more narrowly. Furthermore, model results provide predictions regarding dolomitization timescales and the nature of dolomitizing fluid.

Ferroan dolomite provides a physical link between Latemar platform dikes and dolomitization. This concept may have wider implications related to association of replacement dolomite with igneous intrusions in rifting environments.

## Conflicts of Interest

The authors declare that they have no conflicts of interest.

## Acknowledgments

The authors thank Dr. Alberto Rivas and Dr. Carl Jacquemyn for assistance in the field and the technical staff at KU Leuven and IFP-EN for assistance in the laboratory. They are also grateful to Professor Jean-Marc Baele (University of Mons) for his help with electron microprobe analyses.

## References

[1] H. G. Machel, "Concepts and models of dolomitization: a critical reappraisal," in *The Geometry and Petrogenesis of Dolomite Hydrocarbon Reservoirs*, C. J. R. Braithwaite, G. Rizzi, and G. Darke, Eds., vol. 235, Special Publications, pp. 7–63, Geological Society, London, UK, 2004.

[2] R. S. Arvidson and F. T. Mackenzie, "The dolomite problem: control of precipitation kinetics by temperature and saturation state," *American Journal of Science*, vol. 299, no. 4, pp. 257–288, 1999.

[3] A. M. Wilson, W. Sanford, F. Whitaker, and P. Smart, "Geothermal convection: a mechanism for dolomitization at Enewetak Atoll?" *Journal of Geochemical Exploration*, vol. 69-70, pp. 41–45, 2000.

[4] A. M. Wilson, W. Sanford, F. Whitaker, and P. Smart, "Spatial patterns of diagenesis during geothermal circulation in carbonate platforms," *American Journal of Science*, vol. 301, no. 8, pp. 727–752, 2001.

[5] F. F. Whitaker and Y. Xiao, "Reactive transport modeling of early burial dolomitization of carbonate platforms by geothermal convection," *AAPG Bulletin*, vol. 94, no. 6, pp. 889–917, 2010.

[6] Y. Xiao, G. Jones, F. Whitaker et al., "Fundamental approaches to dolomitization," in *Proceedings of the International Petroleum Technology Conference*, pp. 1–16, 2013.

[7] M. Corbella, E. Gomez-Rivas, J. D. Martín-Martín et al., "Insights to controls on dolomitization by means of reactive transport models applied to the Benicàssim case study (Maestrat Basin, eastern Spain)," *Petroleum Geoscience*, vol. 20, no. 1, pp. 41–54, 2014.

[8] H. Boro, G. Bertotti, and N. J. Hardebol, "Distributed fracturing affecting isolated carbonate platforms, the Latemar Platform Natural Laboratory (Dolomites, North Italy)," *Marine and Petroleum Geology*, vol. 40, no. 1, pp. 69–84, 2013.

[9] P. Gramigna, M. Franceschi, G. Gattolin et al., "Geological map of the Middle Triassic Latemar platform (Western Dolomites, Northern Italy)," *Journal of Maps*, vol. 9, no. 2, pp. 313–324, 2013.

[10] C. Jacquemyn, H. El Desouky, D. Hunt, G. Casini, and R. Swennen, "Dolomitization of the Latemar platform: fluid flow and dolomite evolution," *Marine and Petroleum Geology*, vol. 55, pp. 43–67, 2014.

[11] S. K. Carmichael, J. M. Ferry, and W. F. McDonough, "Formation of replacement dolomite in the Latemar carbonate buildup, dolomites, northern Italy: part 1. Field relations, mineralogy, and geochemistry," *American Journal of Science*, vol. 308, no. 7, pp. 851–884, 2008.

[12] E. N. Wilson, L. A. Hardie, and O. M. Phillips, "Dolomitization front geometry, fluid flow patterns, and the origin of massive dolomite: the Triassic Latemar buildup, northern Italy," *American Journal of Science*, vol. 290, no. 7, pp. 741–796, 1990.

[13] S. K. Carmichael and J. M. Ferry, "Formation of replacement dolomite in the Latemar carbonate buildup, Dolomites, northern Italy: Part 2. Origin of the dolomitizing fluid and the amount and duration of fluid flow," *American Journal of Science*, vol. 308, no. 8, pp. 885–904, 2008.

[14] C. Jacquemyn, M. Huysmans, D. Hunt, G. Casini, and R. Swennen, "Multi-scale three-dimensional distribution of fracture- and igneous intrusion-controlled hydrothermal dolomite from digital outcrop model, Latemar platform, dolomites, northern Italy," *AAPG Bulletin*, vol. 99, no. 5, pp. 957–984, 2015.

[15] R. Mundil, P. Brack, M. Meier, H. Rieber, and F. Oberli, "High resolution U-Pb dating of Middle Triassic volcaniclastics: time-scale calibration and verification of tuning parameters for carbonate sedimentation," *Earth and Planetary Science Letters*, vol. 141, pp. 137–151, 1996.

[16] R. Mundil, J. Palfy, P. R. Renne, and P. Brack, "The Triassic timescale: new constraints and a review of geochronological data," in *Triassic Timescale*, S. G. Lucas, Ed., pp. 41–60, Geological Society, London, UK, 2010.

[17] L. E. Sloman, "Triassic shoshonites from the Dolomites, northern Italy: alkaline arc rock in a strike-slip setting," *Journal of Geophysical Research*, vol. 94, no. 4, pp. 4655–4666, 1989.

[18] A. Rottura, G. M. Bargossi, A. Caggianelli, A. Del Moro, D. Visonà, and C. A. Tranne, "Origin and significance of the Permian high-K calc-alkaline magmatism in the central-eastern Southern Alps, Italy," *Lithos*, vol. 45, no. 1–4, pp. 329–348, 1998.

[19] A. Bosellini, P. Gianolla, and M. Stefani, "Geology of the dolomites," *Episodes*, vol. 26, pp. 181–185, 2003.

[20] J. M. Ferry, B. H. Passey, C. Vasconcelos, and J. M. Eiler, "Formation of dolomite at 40–80°C in the Latemar carbonate buildup, Dolomites, Italy, from clumped isotope thermometry," *Geology*, vol. 39, no. 6, pp. 571–574, 2011.

[21] C. M. Bethke, *Geochemical and Biogeochemical Reaction Modeling*, Cambridge University Press, Cambridge, UK, 2nd edition, 2008.

[22] L. A. Hardie, "Secular variation in seawater chemistry: an explanation for the coupled secular variation in the mineralogies of marine limestones and potash evaporites over the past 600 m.y," *Geology*, vol. 24, pp. 279–283, 1996.

[23] A. Consonni, P. Ronchi, C. Geloni et al., "Application of numerical modelling to a case of compaction-driven dolomitization: a Jurassic palaeohigh in the Po Plain, Italy," *Sedimentology*, vol. 57, no. 1, pp. 209–231, 2010.

[24] T. Gabellone and F. Whitaker, "Secular variations in seawater chemistry controlling dolomitization in shallow reflux systems: insights from reactive transport modelling," *Sedimentology*, vol. 63, pp. 1233–1259, 2016.

[25] J. A. D. Dickson, "A modified staining technique for carbonates in thin section," *Nature*, vol. 205, no. 4971, p. 587, 1965.

[26] M. S. Ghiorso and R. O. Sack, "Chemical mass transfer in magmatic processes IV. A revised and internally consistent thermodynamic model for the interpolation and extrapolation of liquid-solid equilibria in magmatic systems at elevated temperatures and pressures," *Contributions to Mineralogy and Petrology*, vol. 119, no. 2-3, pp. 197–212, 1995.

[27] M. S. Ghiorso, M. M. Hirschmann, P. W. Reiners, and V. C. Kress, "The pMELTS: a revision of MELTS for improved calculation of phase relations and major element partitioning related to partial melting of the mantle to 3 GPa," *Geochemistry, Geophysics, Geosystems*, vol. 3, pp. 1–35, 2002.

[28] J. Moutte, A. Michel, G. Battaia, T. Parra, D. Garcia, and S. Wolf, "ARXIM, a library for thermodynamic modeling of reactive heterogeneous systems, with applications to the simulation of fluid—rock systems," in *Proceedings of the 21st IUPAC International Conference on Chemical Thermodynamics*, Tsukuba, Japan, 2010.

[29] C. Korte, H. W. Kozur, P. Bruckschen, and J. Veizer, "Strontium isotope evolution of late permian and triassic seawater," *Geochimica et Cosmochimica Acta*, vol. 67, no. 1, pp. 47–62, 2003.

[30] P. D. Bons, D. Koehn, and M. W. Jessel, *Lecture Notes in Earth Sciences: Microdynamics Simulation*, Springer, Berlin, Heidelberg, Germany, 2008.

[31] R. G. Berman, "Internally-consistent thermodynamic data for minerals in the system $Na_2O$–$k_2O$–CaO–MgO–FEO–$Fe_2O_3$–$Al_2O_3$–$SiO_2$–$TiO_2$–$H_2O$–$CO_2$," *Journal of Petrology*, vol. 29, no. 2, pp. 445–522, 1988.

[32] M. L. Fuhrman and D. H. Lindsley, "Ternary-feldspar modeling and thermometry," *American Mineralogist*, vol. 73, pp. 201–215, 1988.

[33] C. Meyre, C. de Capitani, and J. H. Partzsch, "A ternary solid solution model for omphacite and its application to geothermobarometry of eclogites from the Middle Adula nappe (Central Alps, Switzerland)," *Journal of Metamorphic Geology*, vol. 15, no. 6, pp. 687–700, 1997.

[34] H. C. Helgeson, D. H. Kirkham, and G. C. Flowers, "Theoretical prediction of the thermodynamic behavior of aqueous electrolytes at high pressures and temperatures: IV. Calculation of activity coefficients, osmotic coefficients, and apparent molal and standard and relative partial molal properties to 600°C and 5 kb," *American Journal of Science*, vol. 291, no. 10, pp. 1249–1516, 1981.

[35] E. L. Shock, D. C. Sassani, M. Willis, and D. A. Sverjensky, "Inorganic species in geologic fluids: correlations among standard molal thermodynamic properties of aqueous ions and hydroxide complexes," *Geochimica et Cosmochimica Acta*, vol. 61, no. 5, pp. 907–950, 1997.

[36] D. A. Sverjensky, E. L. Shock, and H. C. Helgeson, "Prediction of the thermodynamic properties of aqueous metal complexes to 1000°C and 5 kb," *Geochimica et Cosmochimica Acta*, vol. 61, pp. 1359–1412, 1997.

[37] T. J. B. Holland and R. Powell, "An improved and extended internally consistent thermodynamic dataset for phases of petrological interest, involving a new equation of state for solids," *Journal of Metamorphic Geology*, vol. 29, no. 3, pp. 333–383, 2011.

[38] J. L. Palandri and Y. K. Kharaka, "A compilation of rate parameters of water-mineral interaction kinetics for application to geochemical modeling," U.S. Geol. Surv. OPEN FILE Rep 2044-1068, 2004.

[39] W. M. White, *Geochemistry*, Wiley-Blackwell, Oxford, UK, 2013.